Intermontane eolian sand sheet development, Upper Tulum Valley, central-western Argentina

Desenvolvimento do lençol de areia eólica intermontano do Alto Vale do Tulum, centro-oeste da Argentina

Patrick Francisco Fuhr Dal' Bó[1]*, Giorgio Basilici[2]

ABSTRACT: The intermontane Upper Tulum eolian sand sheet covers an area of *ca.* 125 km² at north of the San Juan Province, central-western Argentina. The sand sheet is currently an aggrading system where vegetation cover, surface cementation and periodic flooding withhold the development of dunes with slipfaces. The sand sheet surface is divided into three parts according to the distribution of sedimentary features, which reflects the variation in sediment budget, water table level and periodic flooding. The central sand sheet part is the main area of eolian deposition and is largely stabilized by vegetation. The sedimentary succession is 4 m thick and records the vertical interbedding of eolian and subaqueous deposits, which have been deposited for at least 3.6 ky with sedimentation rates of 86.1 cm/ky. The construction of the sand sheet is associated with deflation of the sand-graded debris sourced by San Juan alluvial fan, which is available mainly in drier fall-winter months where water table is lower and wind speeds are periodically above the threshold velocity for sand transport. The accumulation of sedimentary bodies occurs in a stabilized eolian system where vegetation cover, thin mud veneers and surface cementation are the main agents in promoting accumulation. The preservation of the sand sheet accumulations is enabled by the progressive creation of the accommodation space in a tectonically active basin and the continuous burial of geological bodies favored by high rates of sedimentation.

KEYWORDS: eolian sedimentation; intermontane basin; nebkha; sediment budget; accumulation surface; Holocene.

RESUMO: *O lençol de areia eólica intermontano do Alto Vale do Tulum é uma área em sedimentação de ca. 125 km² desenvolvida ao norte da província de San Juan, no centro-oeste da Argentina. Nesse lençol de areia eólica, a presença de cobertura vegetal, cimentação superficial e inundações periódicas inibem o desenvolvimento de dunas de grande porte com faces de avalhancha. A área de deposição é individualizada em três setores: sul, central e norte e é caracterizada por diferentes processos sedimentares que variam de acordo com a disponibilidade sedimentar, nível do lençol freático e periodicidade de inundações pluviais. A região central é a principal área de deposição e apresenta a maior cobertura vegetal. A sucessão sedimentar nessa área possui 4 m de espessura e mostra alternâncias verticais entre depósitos eólicos e subaquosos, que ocorrem por ao menos 3,6 ka, com taxas de sedimentação de aproximadamente 86,1 cm/10³ anos. A construção do lençol de areia é mantida pela conjunção de fatores que incluem o contínuo suprimento de sedimentos derivados da deflação de depósitos residuais do leque aluvial do rio San Juan, somados a sazonal disponibilidade sedimentar e alta capacidade de transporte dos ventos. A acumulação dos corpos geológicos ocorre associada à atuação de fatores de estabilização da superfície de acumulação, como vegetação, presença de níveis lamíticos e cimentação superficial. A preservação do sistema eólico é favorecida por altas taxas de criação de espaço de acomodação, em bacia tectonicamente ativa, e por altas taxas de sedimentação, que propiciam o contínuo soterramento dos corpos geológicos.*

PALAVRAS-CHAVE: *sedimentação eólica; bacia intermontana; nebkha; saldo sedimentar; superfície de acumulação; Holoceno.*

[1]Laboratório de Geologia Sedimentar, Departamento de Geologia, Instituto de Geociências, Universidade Federal do Rio de Janeiro – UFRJ, Rio de Janeiro (RJ), Brazil. *E-mail:* patrickdalbo@geologia.ufrj.br

[2]Departamento de Geologia e Recursos Naturais, Instituto de Geociências, Universidade Estadual de Campinas – UNICAMP, Campinas (SP), Brazil. *E-mail:* basilici@ige.unicamp.br

*Corresponding author.

INTRODUCTION

Eolian sand sheets are extensive, flat to gently undulating sandy surfaces, covered predominantly with wind ripples and marked by the absence of dunes with slip faces (Fryberger *et al.* 1979; Kocurek & Nielson 1986). Modern eolian sand sheets form significant part of desertic systems worldwide and, although the well-known examples are in trailing and advancing margins of ergs (Fryberger *et al.* 1979), there is a number of examples from coastal, alluvial fan, ephemeral river, and periglacial settings (Hummel & Kocurek 1984; Kocurek & Nielson 1986; Langford 1989; Mountney & Russell 2004). Observations from these modern areas suggest that a number of factors operate single or in conjunction to withhold dune development, including a high water table, surface cementation or binding, periodic or seasonal flooding, significant available population of coarse-grained sediment, and vegetation (Kocurek & Nielson 1986).

In Argentina, several paleoclimatic and geomorphological studies have recognized the vast occurrence of eolian cover during the Holocene. The geomorphology and chronology of dune fields are well established in western areas of San Luis, La Rioja, and San Juan's provinces (Tripaldi & Forman 2007). Presently stabilized and active dune fields are common across the Argentinian Pampas to the Andean Piedmont (Zárate & Tripaldi 2012) and sand sheet deposits appear to form a continuously succession that span most of the Holocene in the San Luis paleodune field (Forman *et al.* 2014). In the Upper Tulum Valley, Suvires (2004) described the influence of eolian sediments as parent materials for soil formation, and Basilici and Dal' Bó (2014) recognized the influence of subaqueous deposition on the construction and accumulation of the eolian sand sheet. However, there is still lack of detailed sedimentological field studies that relates bedform behavior as well as morphology and stratigraphic architecture of the Holocene eolian deposits of western Argentina.

The aim of this paper is to document the sedimentology, internal architecture and geomorphology of a currently active, warm-climate intermontane eolian sand sheet in the Upper Tulum Valley, and to explain its morphology and resulting facies architecture in terms of dynamic interactions between eolian and subaqueous processes from 3.6 ky BP to recent. Furthermore, the construction, accumulation, and preservation of the eolian sand sheet will be evaluated on the basis of the genetic models of Kocurek (1999) and Kocurek and Lancaster (1999) for eolian systems.

GEOLOGICAL SETTING

The study area is situated in the intermontane Upper Tulum Valley (Fig. 1). The Tulum valley, whose extension is about 4,000 km², is a tectonic depression filled with Quaternary alluvial and eolian sediments with several hundreds of meters thick (Lloret & Suvires 2006). This depression is bounded by the Eastern Precordillera to the north and west and by the Pie de Palo range to the east. The area is a rain shadow desert created by a 4,000-m tall Andean Cordillera, which acts as a topographic barrier for the cyclonic circulation from the Pacific.

Fluvial deposits intercalated with windblown sand and loess make up the great part of the Quaternary sedimentary fill of the Upper Tulum depression (Lloret & Suvires 2006). The regime of the rivers in the study area is variable during the years and can be subjected to pluriannual cycles of droughts and floods (Lloret & Suvires 2006), being greatly fed by groundwater springs (Milana *et al.* 2003). Eolian cover is most important at north of the valley, and to the south there is inter-bedding between eolian and *playa* deposits (Suvires 2004).

The source of sediments for eolian transport and deposition is mainly derived from erosion of the sand-sized debris of the San Juan's alluvial fan located *ca.* 45 km to the south of the studied area. The San Juan alluvial fan is characterized by a series of depositional lobes distributed along the San Juan river valley (Fig. 1) that are composed of poorly sorted clasts of sedimentary, plutonic and volcanic rocks derived from western and central Precordillera terrains (Milana & Ruzycki 1999).

The tectonic configuration of the area is dominated by a series of thrust sheets comprising the eastern Precordillera structural province to the west and the thick-skinned Pie de Palo range to the east (Meigs *et al.* 2006). The main tectonic structure is a southeast dipping thrust sheet beneath Precordillera, which is limited at the base on the northwest by the Villicum reverse fault along the range front and on the southeast by the Tulum Valley syncline (Meigs *et al.* 2006). Cambro-Ordovician carbonates of the eastern Precordillera are unconformably overlain by Neogene rocks that comprise the bedrock of the thrust sheet (Fig. 2).

Climate data

The Argentine Meteorological Survey (Servicio Meteorológico Nacional) records annual weather data from this region since 1973 (SMA 2014). The historical climatic data presented here (Fig. 3) is from San Juan's aerodrome weather station located approximately 35 km to the south of the studied area. Based on data from 1973 to 2013, the mean annual temperature is 18ºC, with mean annual maximum and minimum temperatures being 26.5ºC and 13.5ºC, respectively (Fig. 3A). The mean annual precipitation over the period from 1973 to 2013 is 170 mm, and the climate of the area can be classified as arid (Köppen
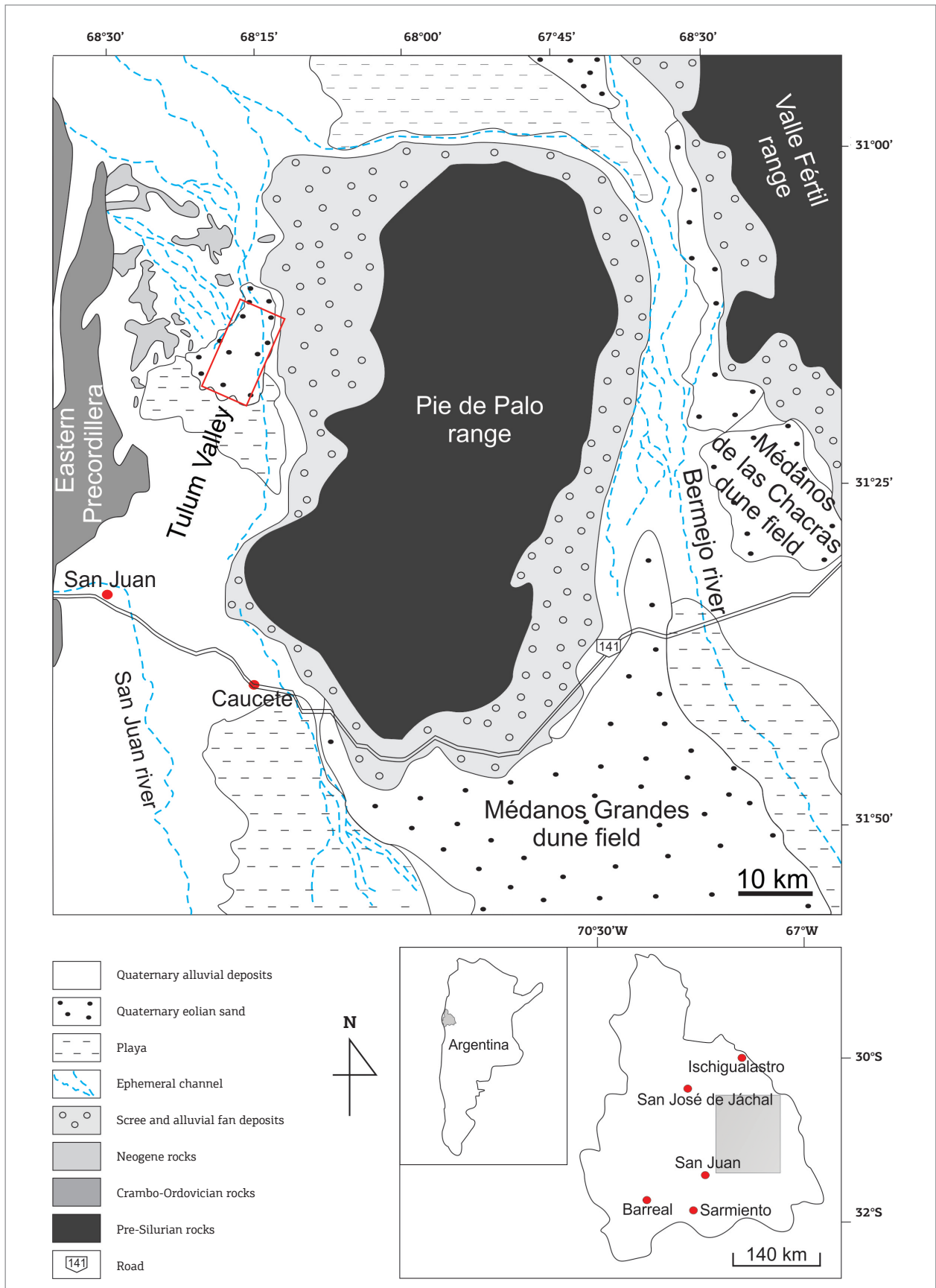
Figure 1. Geologic and geomorphologic map of the Tulum Valley. The rectangle delimits the study area.

1948) (Fig. 3C). The monthly analysis of the last 8-year available climatic data shows a concentration of the rains during the summer months (Fig. 3B) and reveals that more than 40% of the annual precipitation can fall during heavy rains in just a day. The high precipitation indices verified during 2012 winter months is associated to Pacific El Niño Southern Oscillation (ENSO), an important climatic driver which quasi-periodically influences the weather patterns in Central and Northern Argentina and brings increases in temperature and precipitation during late autumn and winter. The hydric balance is negative, where evaporation greatly exceeds precipitation rates. The volume of annual precipitation only accounts for 5% of the total amount of evaporated water (Pereyra 2000). From 1973 to 2013, the mean annual wind speed registered a steadily increase from 2.6 to 4 ms^{-1}, with the increase being the greatest during summer months, when the average wind speed can reach 6 ms^{-1}, with daily peaks by a maximum of 40.7 ms^{-1} (Fig. 3E). In effect, the maximum recorded monthly wind speeds are concentrated during the late spring (October – November) and summer months (December – January) (Fig. 3D). Wind is not a limiting factor for sand movement, considering that the threshold velocity (> 3.76 ms^{-1}) is attained periodically, principally during summer months, when more than 60% of the days are characterized by wind velocities above the threshold (Fig. 3F).

No data regarding wind direction were available from the meteorological station. Tripaldi and Forman (2007), working at Médanos Grandes Dune Field, a small erg located approximately 60 km southeast of the study area, recorded a strongly south to southwesterly component and indicated a resultant drift potential (RDP) to N352, which is in agreement with data recorded from sedimentary structures in the Upper Tulum Valley, indicating sediment transport towards north (Fig. 4).

METHODS

Eolian sand sheet deposits cover ~ 125 km^2 of Upper Tulum surface (Fig. 4). Sand sheet form, distribution, and relationship to the other geomorphologic elements were mapped from Landsat ETM+ satellite images (NASA 2000). Surface observations were conducted along two single transects (Fig. 4). The compartmentalization of the sand sheet into three regions follows these transects (Fig. 4), each of which is characterized by a distinctive set of bedforms and landforms. The transect A-A' is parallel-oriented to the main dry channel that crosses the area and follows the dominant wind direction. This transect allowed the measurement of five stratigraphic sections, each of them with 3 to 4 m thick, exposed in the river banks. The transect B-B' is transversal oriented to the channel section and allowed to verify the lateral extend and distribution of the sedimentary features in relation to bedforms and facies developed inside the channel section.

On the ground, the morphological characteristics of bedforms were evaluated by measuring the length, width, height, crestline orientation, vegetation type and present state of its covering, besides relationship with adjoining
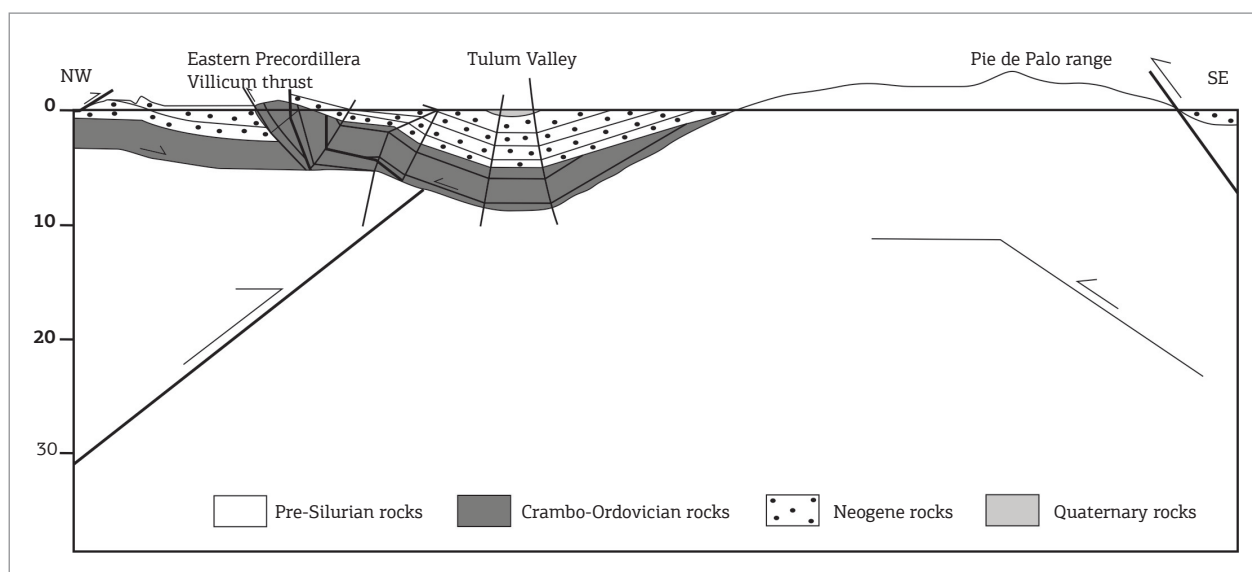
Figure 2. Schematic SE-NW crustal-scale regional profile from Pie de Palo range (southeast) through intermontane Tulum Valley to eastern Precordillera (northwest). Modified from Meigs *et al.* (2006).

A

B

C

D

E

F
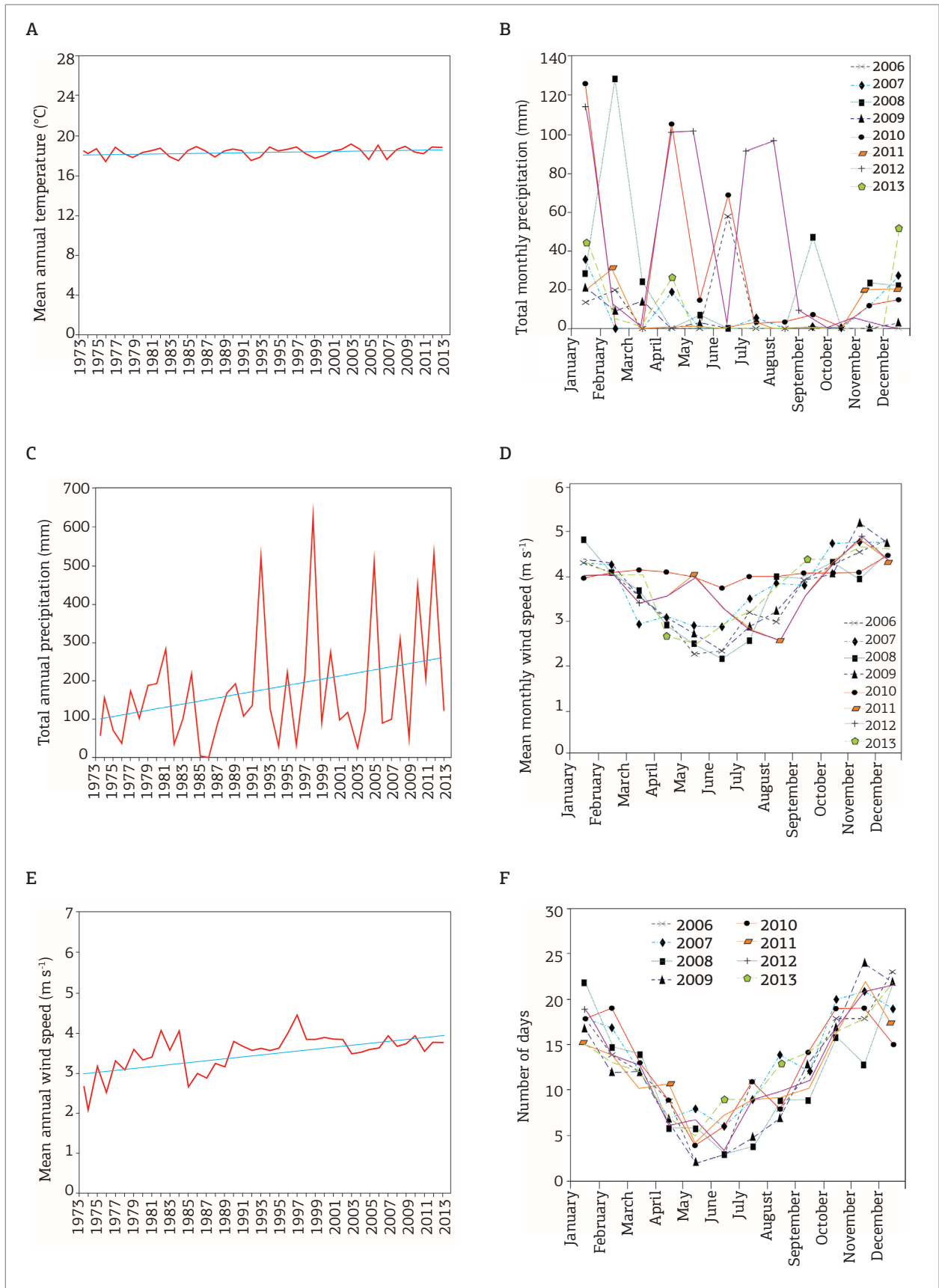
Figure 3. Summary climatic data for the San Juan region (data from weather station San Juan Aero: 31°34'S; 68°41'W).

bedforms or other surface features. To quantify the morphometric parameters of the nebkhas, 50 randomly chosen nebkhas were measured in the vicinities and inside of the dry channel transect. In addition to the surface observations, 16 trenches were dug at 10 sites to ascertain the nature of the internal structure of the bedforms and the preserved stratigraphic record. Trenches attained depths of 0.5 to 1.5 m and extended for up to 5 m, oriented parallel to wind directions and up to 2 m perpendicular to wind directions. The

observation into these trenches was used for the confection of scaled architectural drawings. Sediment samples representative of the main bedform types and deposits were collected from 70 sites across the study area for grain-size analysis.

In a 4-m high bank river section, one sample from the base of the section was taken to optically stimulated luminescence (OSL) dating. OSL analysis was carried out at the Laboratory of Glasses and Dating of the *Faculdade de Tecnologia de São Paulo*, Brazil, using an OSL Automated
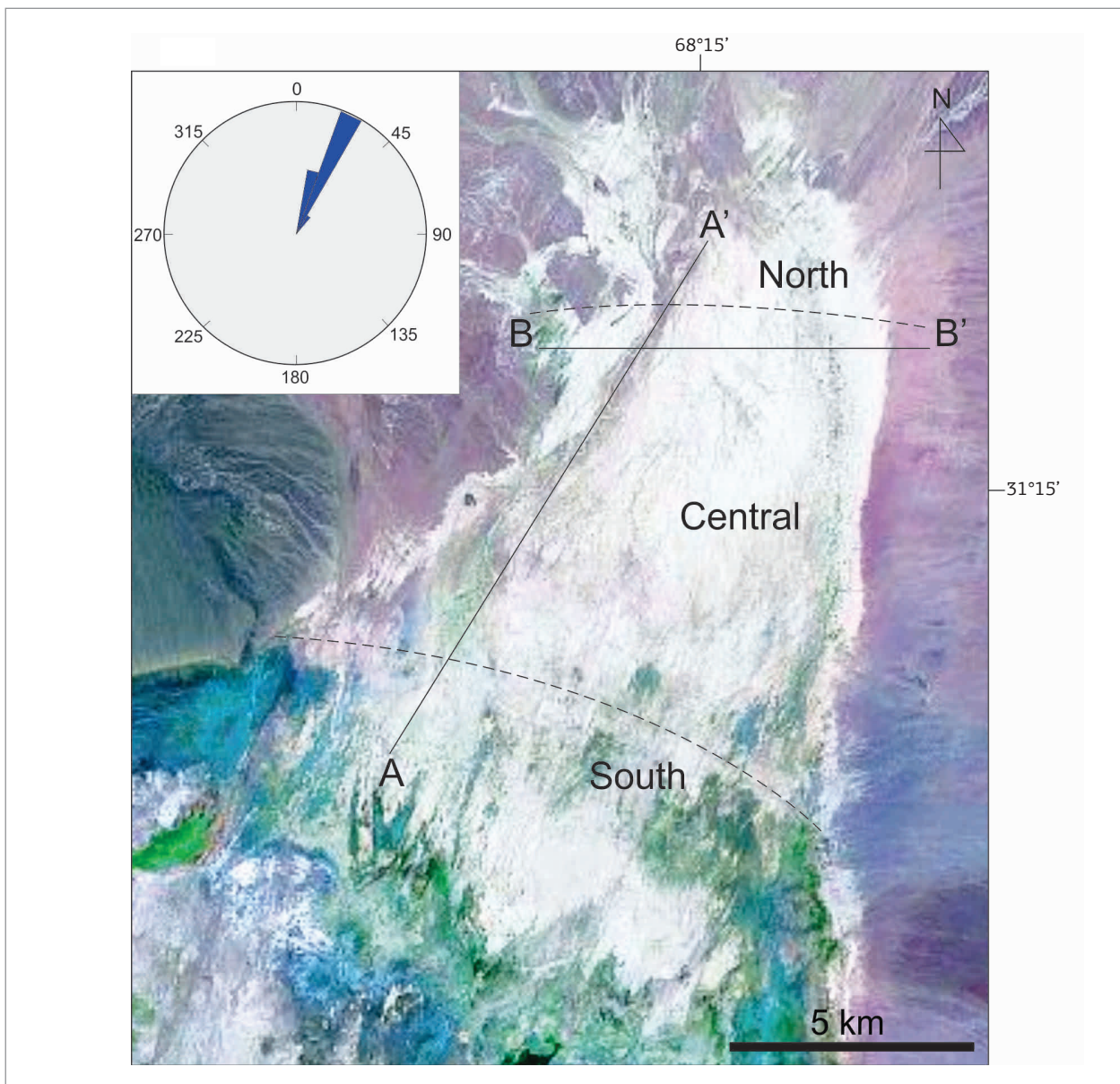
Figure 4. Landsat ETM+ image (bands 7, 4 and 2) of the intermontane Upper Tulum eolian sand sheet. The transect A-A' follows the main dry channel of the study area and the transect B-B' cuts transversally the dry channel section. The sand sheet compartmentalization into south, central, and north regions follows A-A' transect. Wind rose diagram (on the upper left corner) was constructed from measured sedimentary structures and indicates sediment transport towards northeast.

System, model 1100-series of Daybreak Nuclear Instruments. The 0.100 – 0.160 mm quartz fractions were extracted by wet sieving after chemical treatments with HCl (10%), H_2O_2 (20%) and HF (20%), in order to remove carbonates, organic carbon and feldspars, respectively. The gamma irradiation was performed using a ^{60}Co source, and the natural radioactive isotope contents were determined by gamma spectroscopy using a portable inspector spectroscopy workstation, equipped with a NaI(Tl) detector model 802 (Canberra). The optical filter used for OSL dating was Hoya U-340. The equivalent dose (De) was measured using the single-aliquot regenerative (SAR) dose protocol (Murray & Wintle 2000). Dose rates were obtained from the concentrations of U, Th, and K, determined by gamma spectroscopy. The OSL age was obtained by the standardized growth curve (SGC) method. The natural luminescence signal and the laboratory test dose were measured for the SGC (Tab. 1).

COMPONENTS OF THE SAND SHEET ENVIRONMENT

Dry eolian features

Wind ripples are the most widespread dry eolian feature developed in the three regions of the sand sheet. They are present over all the sandy flat surfaces, superimposed on granule megaripples and on upwind side and lateral flanks of nebkha dunes. Wind ripples are characterized by well-sorted to sorted, well-rounded fine-grained sand on ripple stoss and troughs and by sorted to moderately sorted, well-rounded to rounded, fine- to medium-grained sand on ripple crests (Figs. 5A and 5B). The ripple heights vary from 10 to 30 mm and wavelengths are 30 – 100 mm. In plain view, they show straight to few sinuous crest lines. Trenches excavated around low-relief mounds (incipient nebkhas) that are populated by wind ripples showed the dominance of planar horizontal or low-angle laminae (<10°) organized in sets not more than a decimeter thick. Laminae vary in thickness from less than a millimeter to less than a centimeter and laterally may extent for several decimeters. Thinner laminae are enhanced by finer sand covered with iron oxyhydroxide coatings. Inverse-graded strata are observed in thicker laminae, whereas thinner laminae composed of only two or three grains thick shows pin stripe laminations. Gently inclined

foreset laminae can not be distinguished, maybe because of the well-sorted nature of sand grains.

Laterally, sinuous-crested granule megaripples can replace wind ripples (Fig. 6). Granule megaripples are restricted to unvegetated portions of the channel section and are characterized by moderately sorted fine- to medium-grained sand on ripple troughs and by poorly sorted coarse- to very coarse-grained sand and granules on stoss side and megaripple crests (Figs. 5C and 5D). The higher forms attain 50 mm of height, whereas the average height is 30 mm. Upwind slopes are 10° inclined and capped by a variety of volcanic, plutonic, and mud clasts with predominant (~ 70%) mode at 1 phi. Bimodal sediment distribution is evident in the megaripples where the coarsest and poorly sorted grain fractions are concentrated on upper ripple stoss slope and crest, whilst ripple lee slopes and troughs are populated by finer and better sorted sediments. Wavelengths are 0.7 – 1.2 m and the crest lines are oriented N40. The maximum length of the crest line measured in an orientation perpendicular to wind direction is 3 m. Positive correlations between wavelength and coarser grain sizes and wavelength and along-crest line length exist. These forms have an average ripple index (RI = bedform wavelength/bedform height) of 35 and an asymmetry index (stoss slope length/lee slope length) of 2.3. The absence of surface cementation did not enable the complete resolution of the internal structures of the megaripples. Small trenches that were excavated around megaripples, without disrupting the surface arrangement of grains, exposed a non-layered arrangement of fine- and coarse-grained sand and granules without a clear distinction of the foresets.

Nebkha is the only dune form identified in the field. All the dunes are colonized to various extents by shrubs (*Larrea cuneifolia*, *Larrea divaricata*, *Prosopis flexuosa*) and small herbs (*Salicornia perennis*). Vegetation cover occurs on the upwind side of the bedforms, whereas lateral flanks and downwind termination tend to lack vegetation cover. Nebkhas have the long axes oriented N25-40, which is a direction parallel to the prevailing wind direction. They can attain heights of up to 1 m, lengths of up to 13.5 m, and widths of up to 4.5 m. The highest and largest structures are strictly associated with the tallest and denser vegetation.

The nebkhas in the region are typically elongate forms with average width to length ratio of 0.40. Fig. 7A shows a strong positive correlation between dune length and width

Table 1. Optically stimulated luminescence age obtained for Upper Tulum eolian sand sheet.

Sample	Th (ppm)	U (ppm)	K (%)	Annual dose rate (μGy/yr)	Accumulated dose (Gy)	Age (years)
LSA	10.493	2.266	0.133	1,650 ± 60	6.0	3,600 ± 310
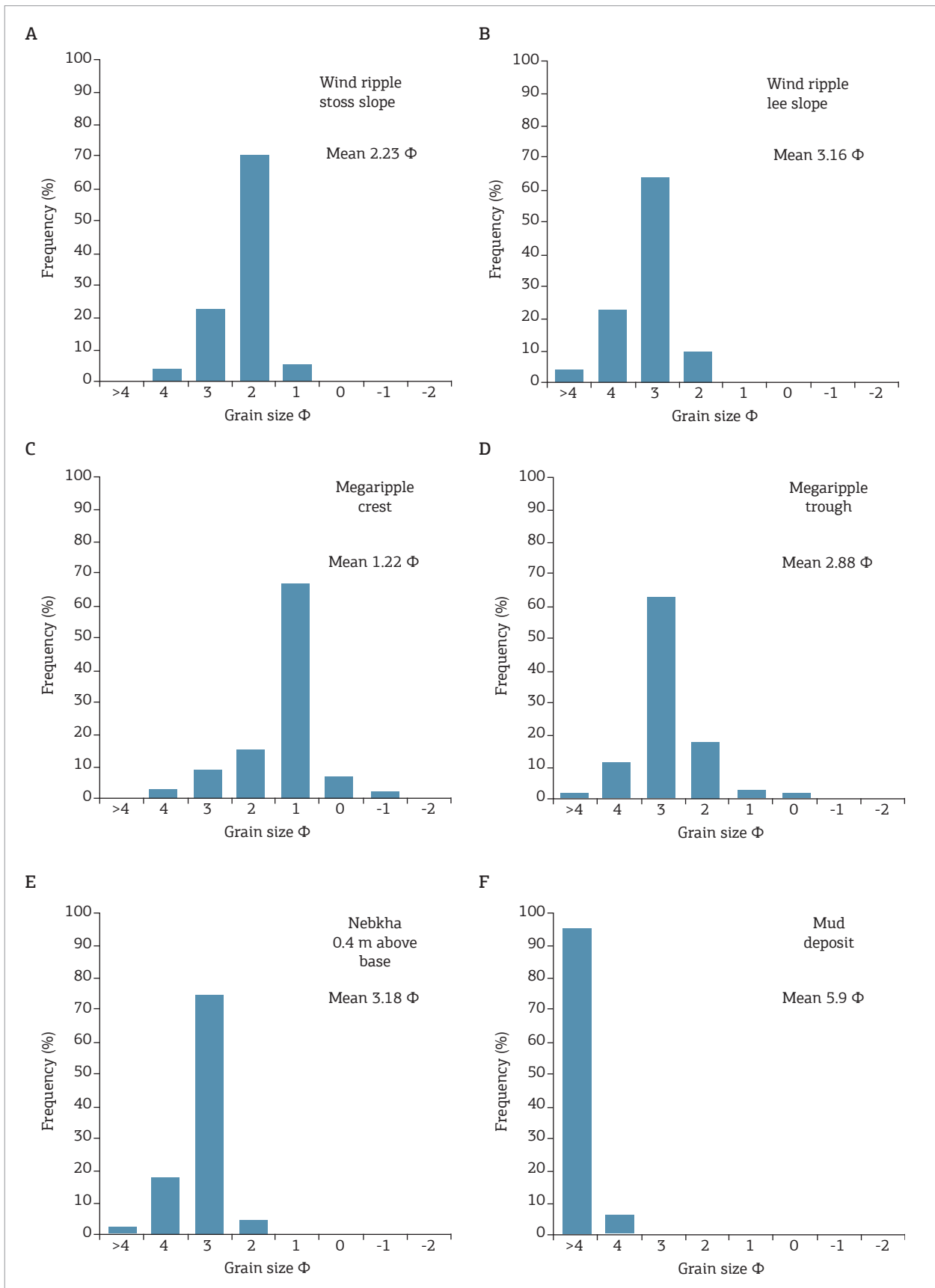
Figure 5. Grain size data.

(r = 0.86); the solid line shows a linear trend between these two measured parameters at a high significance (R² = 0.71). The data scattered in this plot principally reflects local variation in vegetation cover, as plant morphology, distribution and density. The dunes are not large forms, only one dune attains 1 m of height, and the average height is 0.34 m. A direct relationship between dune length and height is shown in Fig. 7B; it has a strong positive correlation (r = 0.85) and a determination coefficient (R²) estimated to be 0.72, attesting that a linear trend between the variants fits the data very well.

Horizontal component (L) of the dune is the mean of length (l) and width (w) of the dune; thus, L = (l + w)/2. For the 50 measured nebkhas, the height increases with the increase in the horizontal component (Fig. 7C). Different orders of polynomials were tested, and it was found that the two-order polynomial fits better the data as follows:

$$H = A \cdot L^2 + B \cdot L + C$$

where H is the dune height, L is the horizontal component, A, B, and C are constants. Although the linear function fit is also significant, the polynomial function shows a relative better fit (1.3%, R² = 0.74), with a positive correlation of 0.86. The ratio between the height and horizontal component of 1/8 indicates flattened forms.

The most developed nebkhas occur along the transect A-A', in the central sand sheet part, where two or three nebkhas have grown together to form amalgamated dunes by lateral linking and merging. Lateral and lower dune flanks are entirely populated by wind ripples, and the resulting grain size characteristics are very similar to the wind ripples (Fig. 5E).

Erosional features such as yardangs only occur in the north part of the sand sheet. These linear wind-abraded erosional forms are developed on sand-cemented wind ripple deposits (Fig. 8) and attain a maximum height of 0.8 m. The morphometric parameters of these forms have revealed a ratio of length, width, and height of 5.4 : 2.2 : 1.0. They have long axes oriented ~ N20, parallel to the prevailing southerly winds.

Interpretation

Wind ripples and megaripples are the most common dry eolian features described in the Upper Tulum eolian sand sheet and in another eolian sand sheet environments elsewhere (Kocurek & Nielson 1986; Fryberger *et al.* 1992; Mountney 2006).

The basic difference between ripples and megaripples lies in the relative magnitudes of the wind strength and the size of the crest grains (Bagnold 1941). In the case of ripples, regular winds are strong enough to remove the topmost crest grains whenever the crest height reaches a certain limiting height. In the megaripples, the coarsest grains that accumulate at the crest are too large to be removed by average winds, except by occasional strong winds. Bagnold (1941) also suggested that the conditions necessary for the growth of megaripples are
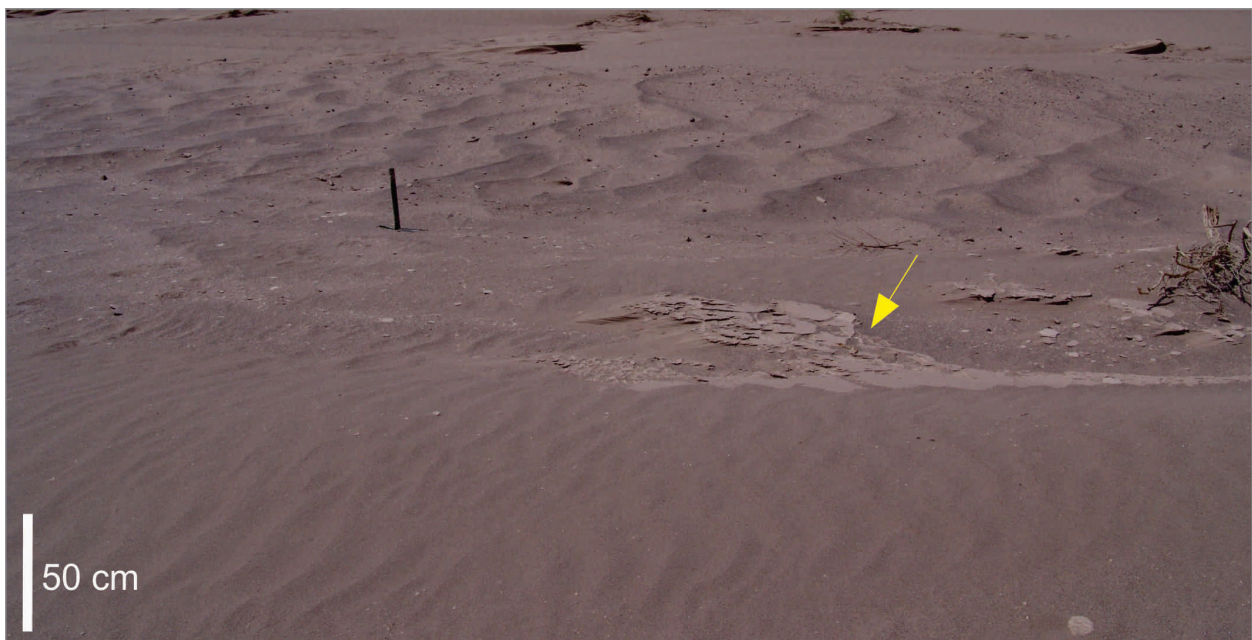
Figure 6. Oblique view showing wind ripples in the foreground and megaripples in the background. The arrow shows a thin layer of mud deposits.

1. availability of sufficient coarse grains which have a diameter 3 – 7 times larger than the mean diameter of grains in saltation,
2. a constant supply of fine sand in saltation to sustain forward movement of the coarse grains by creep, and
3. wind velocity below the threshold to remove coarse grains from the megaripple crest.
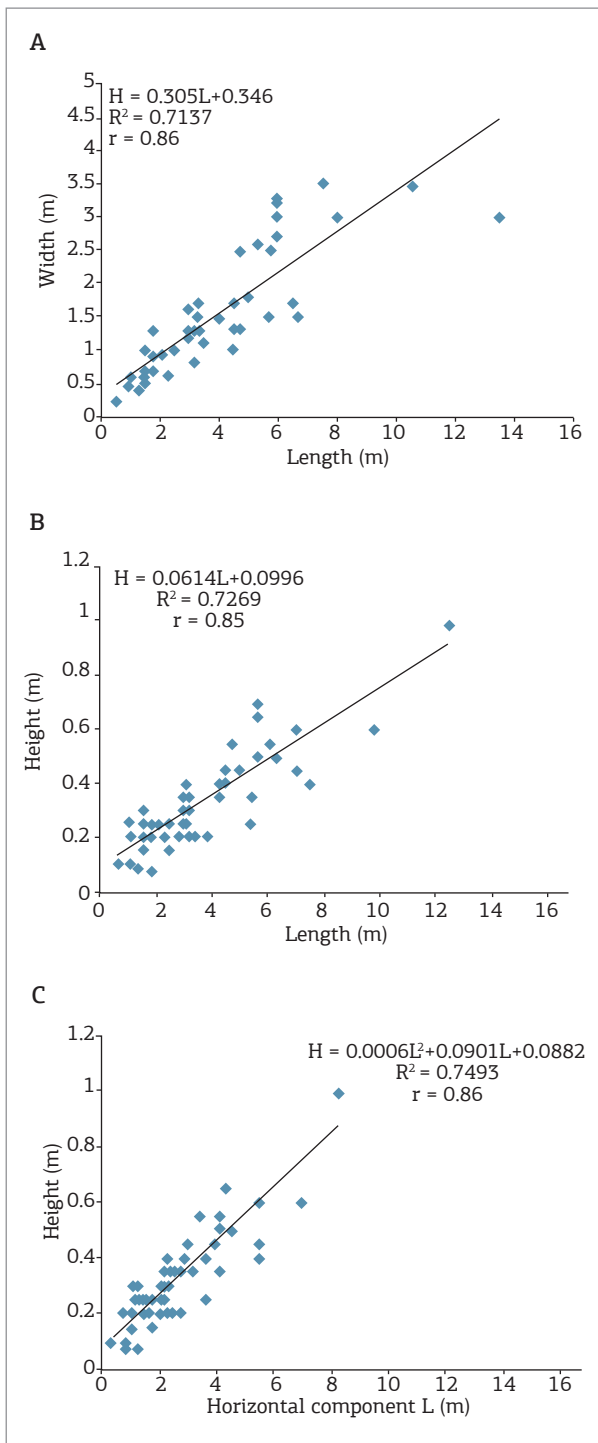
The positive correlation between wavelength and grain size suggests that the formation of these bedforms are connected to saltation or reptation path length, where minor surface perturbations act as the catalyst required to initiate ripple development (Anderson 1987). Several studies suggest that granule megaripples form common wind ripples (Fryberger *et al*. 1992 and references therein). The larger size and spacing of these forms are related to higher wind speeds that enhance the saltation and reptation path length and probably are associated with topographic depressions, which promotes wind deceleration and expansion, thus enhancing accumulation. On daily wind peaks during the study, sediment grain transport over the megaripples was active and comprised a combination of grain creep, saltation and reptation. Milana (2009) called these small megaripple forms described herein of small-scale gravel ripples, where the term large-scale gravel ripples is restricted to bedforms reaching 43 m in wavelength and 2.3 m in height.

Deposits of coarse-grained or granule megaripples are characterized commonly by inverse grading with or without development of coarse-grained foresets (Clemmensen & Abrahamsen 1983). In the studied megaripples, there was not a clear distinction of coarse-grained foresets, and the deposits show a non-layered, irregular distribution of fine- and coarse-grained sand, resulting in deposits with a poorly sorted texture, similar to those described by Fryberger *et al*. (1992) around megaripple fields of central-west Namibia. This texture results from an admixture of fine sand that fall among the spaces between the coarse sand and granule during deposition and from the fine sand collected in the ripple troughs at the surface.

The internal architecture of incipient nebkhas (embryonic state) dominated by wind ripples revealed planar or low angle parallel strata which have formed by wind ripple migration on a flat or gently undulatory sandy surface and have been preserved by subcritical climbing (Hunter 1977). The pin stripe lamination is also characteristic of wind ripple deposits (Fryberger & Schenk 1988). According to Sharp (1963), the active short-lived ripples tend to develop on sandy surfaces that are in a state of relative equilibrium or slow deposition, while surfaces experiencing marked erosion or vigorous deposition generally do not display ripples.

The internal stratigraphic architecture of five nebkhas (mature state) was examined by digging 0.5 to 1 m deep and 1 to 3 m wide trenches oriented at a variety of angles around the bedforms. The distribution of sedimentary strata, their orientation to the prevailing wind direction, their bounding surfaces, and other biological features are recorded in architectural drawings (Fig. 9).

Figure 7. Morphometric parameters of the nebkhas.

The low angle of much of the strata and bounding surfaces in the lower parts of dune cores indicates that these bedforms initiated as low-relief mounds. The broad spread of low angle strata azimuths reflects the dome-shaped form of the dunes and signifies bedform growth on east, north and west facing flanks, probably in response to a prevailing southerly wind. Planar or low angle laminae are the depositional product of wind ripple migration and have been preserved by subcritical climbing (Hunter 1977).

Major bounding surfaces represent episodes of dune stabilization, and their convex-up geometries oriented parallel to the wind direction reflect the dome-shaped form of the dunes at various stages in their development. The minor bounding surfaces are reactivation surfaces, generated by local scouring of the dune flanks, probably in response to storm events and short-lived changes in wind direction (Rubin 1987).

We did not identified grainfall strata as described by Mountney and Russell (2009) in nebkhas of the same structure. Kocurek *et al.* (1992) pointed out that the transition from "protodunes" dominated by wind ripples to "protodunes" with a grainfall strata involves necessarily an upwind slope inclined of at least 10° and a lee slope with an angle of about 22°, which promotes the change from a flow expansion to a complete flow separation, and, once separation occurs, wind speed at the base of the lee slope falls to near zero, promoting the deposition of thin fine-grained grainfall strata. In the sectioned dunes, the angle of upwind slope was about 3 – 5° and the downwind angle never surpassed 10°.

The presence of vegetation is essential to the nucleation, growth, and stabilization of nebkhas (Tengberg & Chen 1998). Even in settings characterized by airflows that are undersaturated with respect to their potential sediment carrying capacity, nebkhas are able to grow, as long as the surface of the dune remains colonized by vegetation (Mountney & Russell 2006). In particular, the effectiveness of various species of *Larrea* and *Prosopis* as an agent to reduce near surface wind velocity is crucial to the sand trapping and their root mats are essential to the sand stabilization that enables long-term nebkha growth (Tengberg & Chen 1998; Langford 2000). The preferential development of larger nebkhas within the dry channel results exclusively from the localized disruption of airflow induced by vegetation (Mountney & Russell 2006) because wind contraction and acceleration are intensified as the airflow is funneled between channel banks (Mountney & Russell 2004). The increased frequency of small nebkhas along the base of terrace slopes probably reflects the development of a separation cell as the airflow rises up the channel banks and over the terrace slope (Mountney & Russell 2006). Progressively away from the base of terrace (following transect B-B'), dunes show a reduction in size and frequency as the airflow reattaches and the transport capacity of the wind is locally increased.

Yardangs found in the north part of the sand sheet were classified as micro-yardangs (Goudie 2007), and their occurrence suggests local deflationary conditions where the wind is undersaturated with respect to sediment load (Kocurek & Havholm 1993). The well-developed wind-abraded lateral surfaces of yardangs oriented parallel to the prevailing wind direction indicate that sediment transport towards the northeast has been ongoing for a considerable time. Although the rates of yardang formation and development are still poorly known, some quantifications have shown that small yardangs may form in less than 2000 years (Laity 1994).
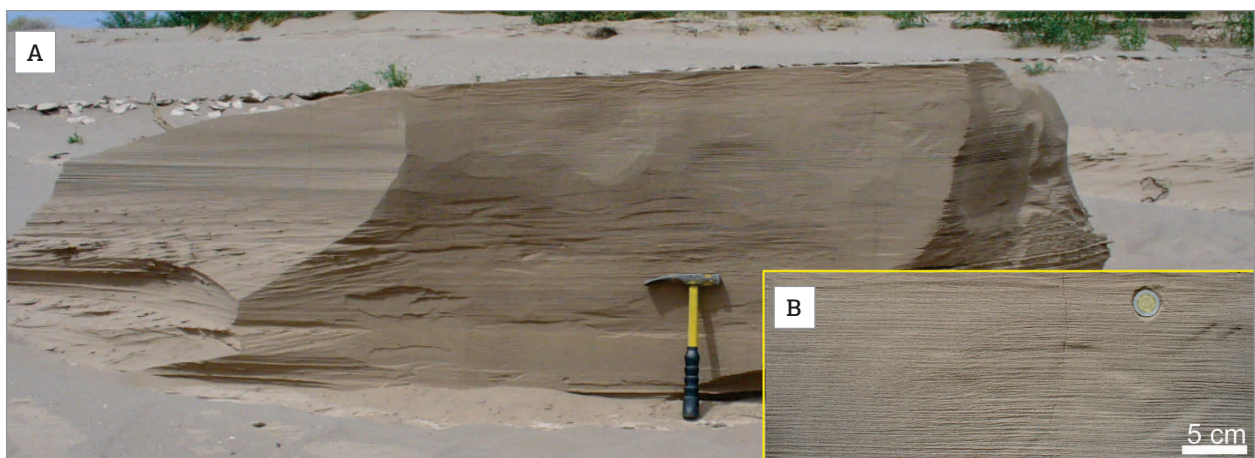
Figure 8. Yardang. (A) Wind-sculptured micro-yardang form developed on wind ripple deposits. (B) Detail of the deposits showing very fine- to fine-grained sandstone with inversely graded wind ripple strata. The hammer is 0.34 m long.

Damp eolian features

In the area close to the south extremity of the sand sheet (transitional area from sand sheet to *playa* environment), where the surface is periodically damp, a variety of adhesion features are found, including adhesion ripples, adhesion warts, and evaporitic-adhesion structures (Kocurek & Fielder 1982; Olsen *et al.* 1989; Goodall *et al.* 2000). Adhesion ripples and warts are small structures, 0.3 – 2 mm high, less than 5 mm in wavelength, characterized by very fine- to fine-grained sand adhered to the damp surface. These structures form small undulations randomly distributed on the depositional surface, with discontinuous crest lines crudely oriented transversal to
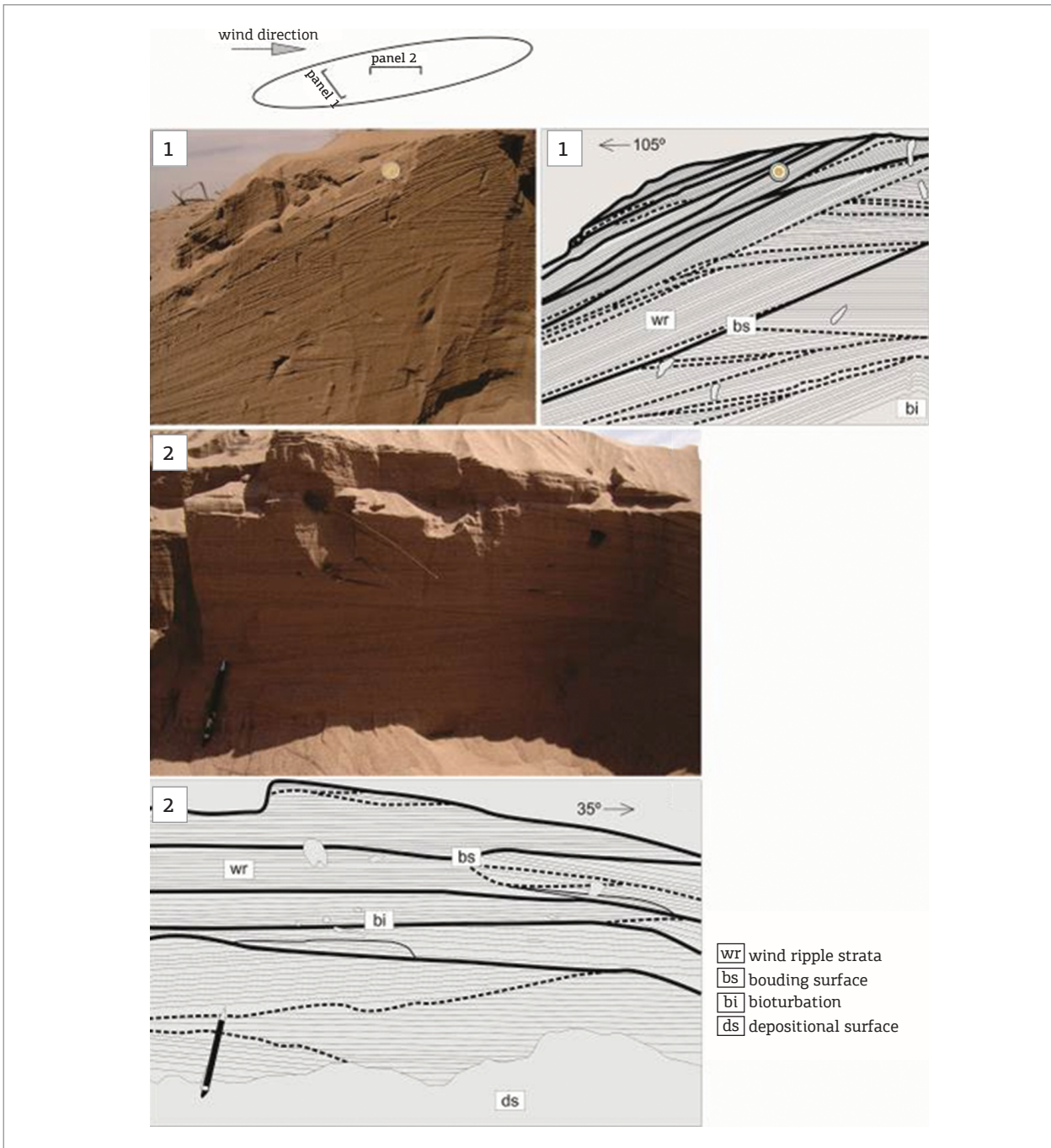
Figure 9. Internal sedimentary architecture of a nebkha. Panel 1 is oriented perpendicular to the wind direction and panel 2 is oriented parallel to the wind direction. Solid lines represent major bounding surfaces and dashed lines, minor bounding surfaces. The coin for scale is 20 mm in diameter, and the pencil is 0.14 m long.

the wind direction. Evaporitic-adhesion structure forms irregular surface reliefs < 30 mm in high, in which high proportion of sand and silty mud grains is adhered to the hygroscopic damp surface of salts (Fig. 10A). This structure exhibits a characteristic wrinkled morphology and a bicolored pattern, formed by differentiations between dark adhering sand and silty mud grains and white salt crusts.

Soft sediment deformational structures are more common in sediments at the south margin of the sand sheet, but they can also occur in sections located in the central part. Sets composed of deformed laminae, 0.1 – 0.3 m thick, are common in the middle and upper portions of the

Figure 10. Damp eolian features. (A) Evaporitic-adhesion structure in plain view. The topographic surface is wrinkled and shows the bicolored pattern typical of this structure. (B) Small-scale deformation on wind ripple deposits. Contortion and disruption of the laminae evidence liquefaction at or close to the depositional surface.

wind ripple deposits. The lower surface of the deformed sets may have sharp to gradational contacts and is underlain by undeformed low angle wind ripple deposits. The deformed sets may extend laterally for up to 1 m. In cross section, the deformational structures are characterized by small contortions, convex-up and isolated concave-up forms due to folding and disruption of the horizontal wind ripple laminae (Fig. 10B). Despite the magnitude of deformation, the parallel horizontal strata remain unbroken in some parts of the sections, and the primary sedimentary structures are still evident.

Interpretation

The adhesion of grains transported by the wind to damp surfaces results in the generation of adhesion structures (Kocurek & Fielder 1982; Olsen *et al.* 1989). Formation of adhesion structures requires high substrate moisture (> 80%), and growth can only take place as long as moisture is drawn to the surface by capillary action (Kocurek & Fielder 1982). These structures are characterized by low-relief ridges and the accretion of saltating grains to the upwind side of the ripples generates a slightly convex inclination of the crests to the upwind direction. Adhesion warts have a more random distribution than adhesion ripples and probably are associated to roughly nature of the substrate and frequent changes in wind direction (Kocurek & Fielder 1982; Olsen *et al.* 1989).

Evaporitic-adhesion structure is the largest adhesion structure observed, and its formation is associated to the presence of surface salts. The conspicuous occurrence of this structure on the depositional surface at the south extremity of the sand sheet suggests a high water table in this region. The formation of surface evaporites may follow two main processes, efflorescence and precipitation. Efflorescence of salt crystals occurs where salt accumulates by direct crystallization onto sediment grains as a result of the evaporation of saline ground water adhering to those grains, and precipitation forms by the evaporation to dryness of ephemeral ponds of rainwater (Goodall *et al.* 2000). The adhesion of sand and silty mud to salt crystals occurs by the hygroscopic action of evaporites (Kocurek & Fielder 1982), and the bicolored pattern seen on the surface of this structure is given by the high proportion of adhering dark windblown dust on white salt crystals. The ground water in the Upper Tulum Valley is enriched in saline compounds such as sodium chloride and calcium sulphate (Lloret & Suvires 2006).

The limited extent of the small-scale deformation and its occurrence in the middle to upper parts of the wind ripple strata indicate that folding and disruption of the horizontal laminae developed by liquefaction near the depositional surface. Liquefaction results from an elevation of pore-water pressure
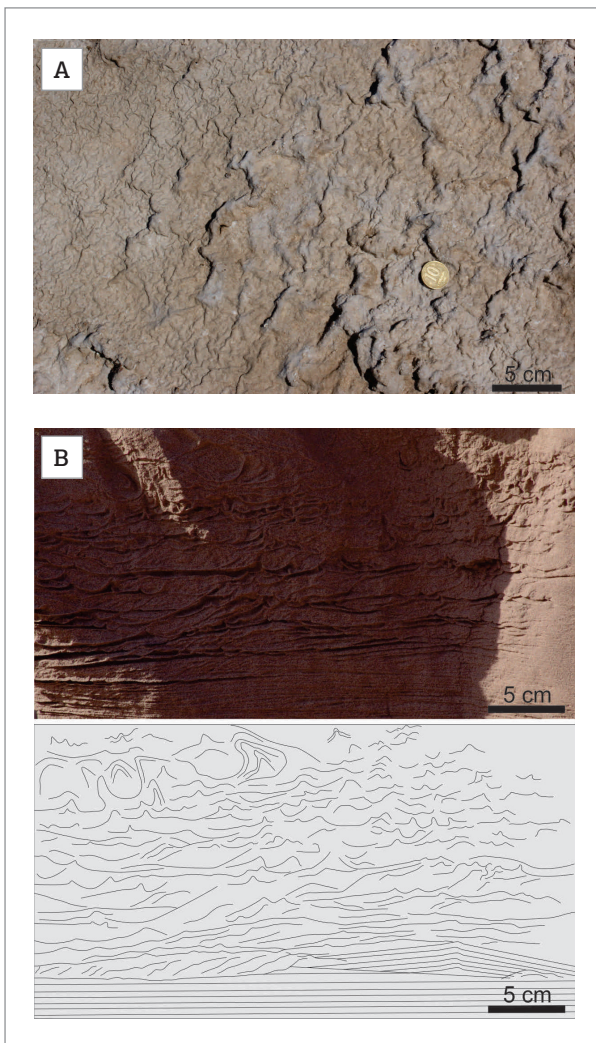
as the wetting front infiltrates into highly porous eolian sands (Mountney 2006). The tightly packed wind ripple laminae are susceptible to liquefaction by collapse of grain packing due to mechanical loading (Mountney & Thompson 2002).

The vertical transition between dry to damp eolian features reflects changes in the substrate wetness possibly associated to minor fluctuations in the ground water level, resulting from seasonal weather variations (Mountney & Thompson 2002), small-scale climatic variations (Kocurek & Havholm 1993), or episodic interdune flooding (Lancaster & Teller 1988; Langford 1989).

Subaqueous features

Two types of subaqueous sedimentary features are noted in the sand sheet area: current ripples and mud layers. Both features are developed in the three regions of the sand sheet.

Current ripples are the most conspicuous subaqueous feature observed. They occur on depositional surface and in trenches excavated in the areas affected by flood deposition. They are characterized by well-sorted to sorted, rounded fine-grained sand, organized in sets 10 to 50 mm thick, which have a lateral continuity of more than 1 m. Ripples are asymmetrical, have straight crest lines and show foreset azimuths oriented N210-250. The heights vary from 10 to 20 mm and wavelengths are 90 – 180 mm. The ripple cross laminae are formed by inclined foresets with dip angles

typically around 20°, which, in some cases, show climbing laminae with preserved form sets. Current ripples abruptly overlie wind ripple strata and are overlain by thin silty mud deposits (Fig. 11).

Mud deposits are composed by more than 90% of the grain size distribution > 4 ϕ (Fig. 5F). They cover almost the entire sand sheet surface and show differentiations between thicker and continuous layers and thinner and reworked portions that are associated with wind deposits (Fig. 12A). The deposits are 10 to 150 mm thick and exhibit an irregular and cracking pattern on surface and an undulatory to roughly lenticular shape in cross section. The surface cracking is marked by polygonal fractures, 20 to 100 mm in diameter, filled with fine-grained eolian sand, and shows rain drop impressions (Fig. 12B). These muddy deposits also constitute an important source of low-density clasts that are transported by the wind and form a significant part of the granule mode of the megaripples. In natural sections, 0.6 m thick, it is possible to observe the occurrence of several mud layers interbedded with wind ripple strata (Fig. 12C) and mud flakes within wind ripple strata.

Interpretation

The presence of current ripples and mud deposits in an eolian setting suggests water-driven processes (Ahlbrandt & Fryberger 1981; Kocurek 1981; Kocurek & Nielson 1986;

fd flood deposits
sc surface cracking
sbr subaqueous ripple strata
bs bounding surface
wr wind ripple strata
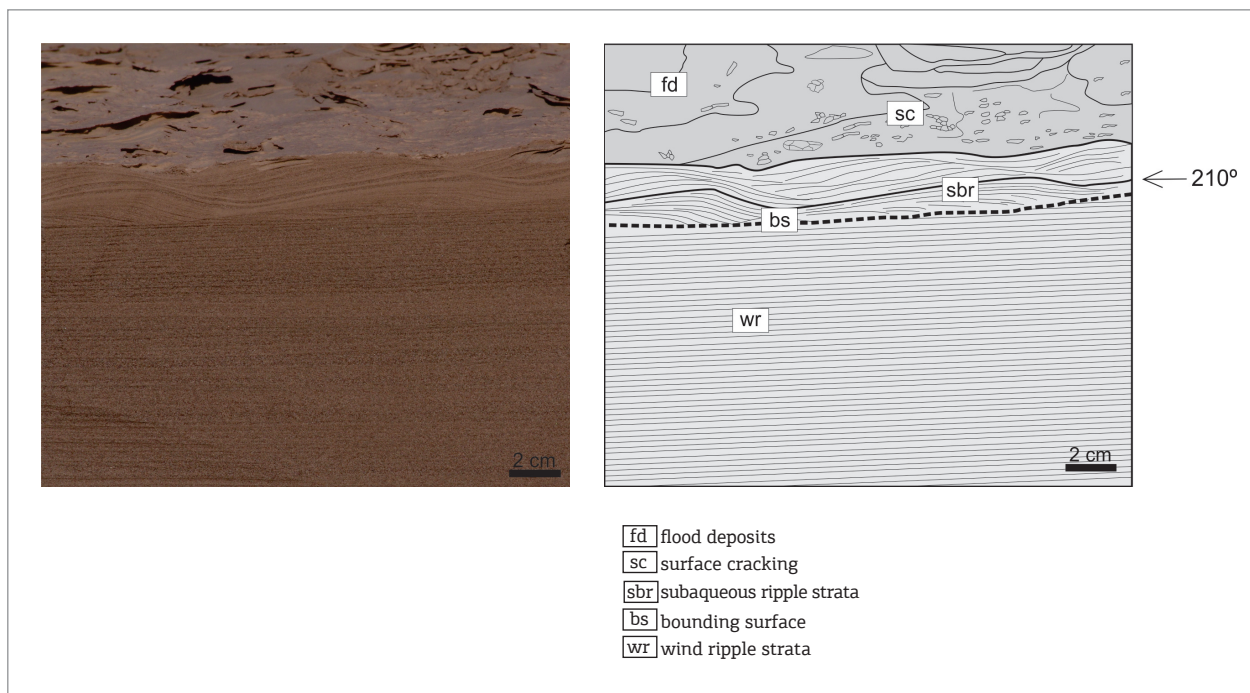
Figure 11. Subaqueous sedimentary features showing the vertical transition from wind ripple strata to subaqueous ripple strata which are overlain by silty mud deposits.

Lancaster & Teller 1988; Langford 1989; Langford & Chan 1989; Kocurek *et al.* 1992). Current ripples characterized by straight crest lines indicate water flow conditions at low velocities and were primarily associated with upper sequences of wadi deposits (Glennie 1970), whereas mud deposits suggest stagnant waters in interdune settings (Glennie 1970; Ahlbrandt & Fryberger 1981; Mountney & Russell 2006).

A dry river channel crudely oriented at north-south direction crosses the study area (transect A-A'). The morphological characterization and sedimentological analysis of five stratigraphic sections insight the river channel have revealed that most of the sedimentary facies are the product of wind deposition, and other sedimentary facies or subaqueous structures that support a fluvial origin for the described deposits were not observed.

Kocurek (1981), working in the Jurassic Entrada Sandstone Formation, Utah, described an array of subaqueous sedimentary features in interdune deposits characterized by the absence of channel systems. Based on observations carried out in a modern sand sheet adjacent to the dune field of Padre Island, Texas, Kocurek (1981) found an analogous situation and interpreted those water-laid deposits as a depositional product of ephemeral shallow floods associated with heavy rains. Similarly, Langford (1989) described several layers formed by couplets of subaqueous climbing ripples overlaid by
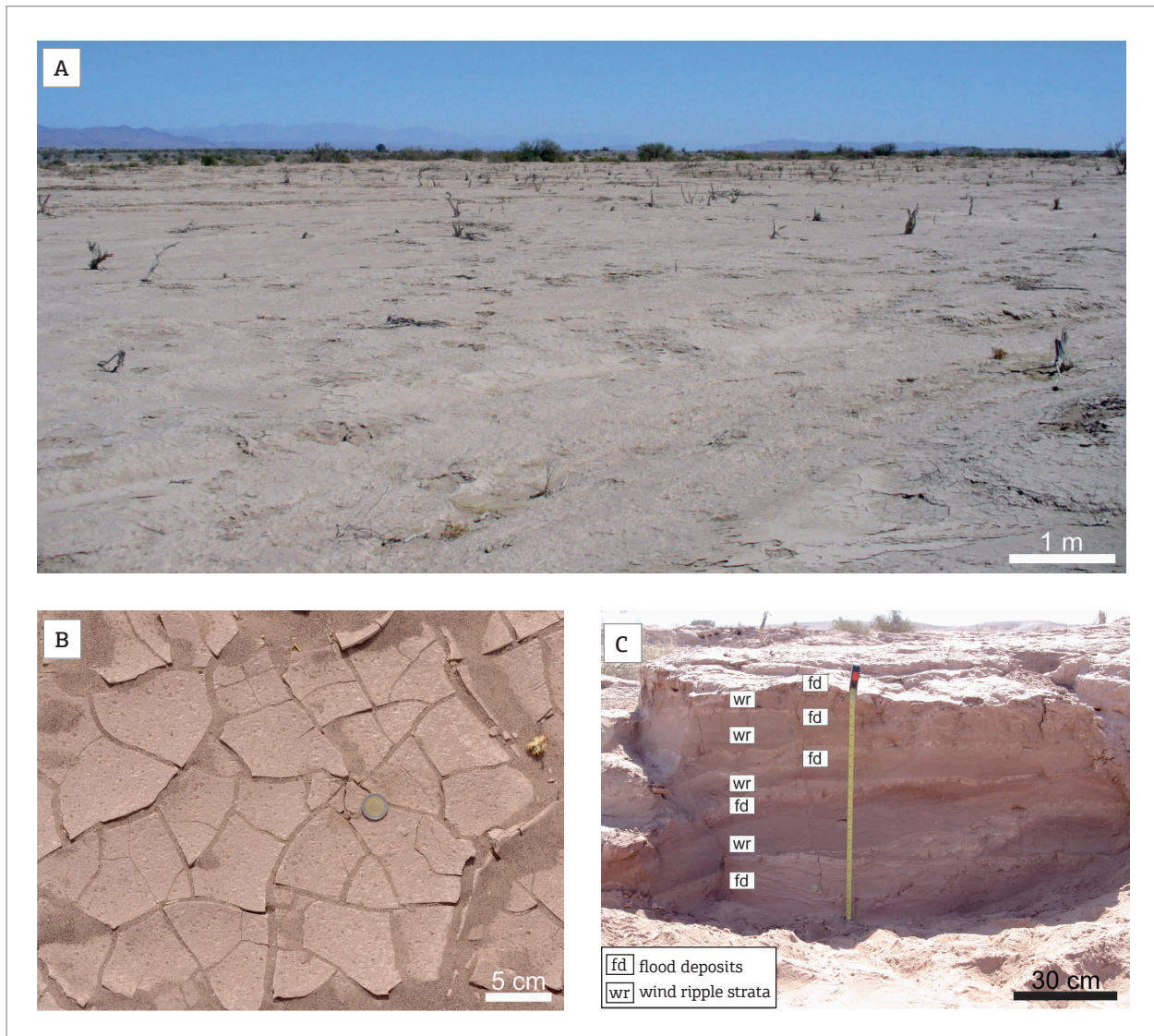
Figure 12. Flood deposits. (A) Irregular and newly formed depositional surface after rainwater flooding. (B) Desiccation cracks filled with eolian sand. (C) Natural exposure showing the vertical interbedding of flood deposits and wind ripple strata.

mud deposits in the Mojave River Wash area, California, and interpreted those features as shallow water rework of eolian sands produced by floodwaters, where climbing structures indicate rapid deposition followed by short periods of stagnant water.

A flash flood can be generated in a desert environment during or shortly following a rainfall event, especially when the rain is of high intensity (Lancaster & Teller 1988). The analysis of historical climatic data available for the Tulum Valley showed that precipitations are concentrated in the summer months and that extreme rainstorms are prone to occur in the area. Probably, the high concentrated precipitation events enhanced the surface runoff around the sand sheet area and the sediment is carried through the depositional surface in unconfined flows to very shallow channels unable to generate large sedimentary structures.

Rainwater flooding is also an important agent in the formation of depositional surfaces. Following a rainy period during January, the authors visited the area and observed that most of the eolian bedforms were covered by subaqueous deposits and that much of the substrate was characterized by straight-crested current ripples and thin mud deposits.

DISCUSSION AND CONCLUSIONS

The Upper Tulum eolian sand sheet is an example of an intermontane eolian system where vegetation cover, surface cementation, and periodic flooding are the main controlling factors for sand sheet development. The eolian sand cover is in excess of 4 m of thickness and the stratigraphic record displays a set of dynamic interactions between eolian and subaqueous processes, which have been ongoing for at least ~ 3.6 ky with an average sedimentation rate of 86.1 cm/ky (Fig. 13).

Water fluxes driven by heavy rains generated subaqueous deposits which have been frequently modified by wind action. The subaqueous deposition formed subaqueous current ripple strata and is accompanied by a thin layer of mud sediments. The mud sediments act to blanket the surface, thus protecting underlying eolian sand from deflation and also sources mud clasts to megaripples development, when the surface is completely dry.

The periodic changes in available water content are also responsible for the modification in the configuration of the morpho-depositional surface. During the dry season (July – October), the surface is little affected by water fluxes, and the near flat-lying depositional surface is mantled by deposits of loose sand-grade wind ripples and granule-grade megaripples. Just after a rainy day, the surface can exhibit a different aspect and the sedimentary structures that were forming as

a consequence of sand-free movement can change to subaqueous deposits at the north and central and small adhesion structures controlled by the temporally rise of the water table at the south of the sand sheet.

According to Kocurek and Lancaster (1999), eolian bedform construction occurs as a consequence of bedform growth upon a depositional surface. Construction demands the generation of a suitable upwind amount of sediment supply, the availability of that supply for wind transport and a spatial reduction in sediment carrying capacity of the wind.

Ongoing sand sheet construction is possible because San Juan alluvial fan sources sand-grade sediments to the sand sheet surface. This sediment is entrained and transported across the sand sheet by south and southwesterly winds, which periodically exceed the threshold velocity required for sand transport. From morphological observations, it was evident that the surface roughness plays an essential role for the potential sand deposition. All initial depositional sites are related to elements of surface roughness, from grasses to small trees. Deposition of sand has occurred close to roughness elements possibly because of a conjunction of two factors that include local lowering of the wind transport capacity caused by deceleration of the wind and formation of secondary airflow patterns around obstacles (*i.e.* shadow effect) and as a consequence of an impediment to grain movement itself caused by direct collisions to obstacles. The larger plants are the most effective sand traps, and following construction is enhanced by root mats, which act as a binding agent on upwind dune slopes. The availability of sediments is controlled in the source area by periodical changes in the level of the water table. Most of the sediments are sourced by alluvial fans during summer months, contemporaneous input-availability limited (CI_{AL}), in the terminology of Kocurek and Lancaster (1999); however, they are only available to wind erosion and transport during winter months, when the lowering of the water table enables sand sheet building (lagged influx-availability limited — LI_{AL}). The presence of stabilizing agents on sand sheet surface (*e.g.* thin mud veneer, vegetation cover, and salt crusts) accounts for the contemporaneous input — CI_{AL}, prevents cannibalization of the deposited sediments and enhances accumulation of sedimentary strata in a stabilizing eolian setting (Kocurek & Havholm 1993).

The stabilizing influence of surface elements has been responsible for accumulation to the taken place. The airflow is undersaturated with respect to its potential sand carrying capacity in much of the year and across the sand sheet surface. The ubiquitous presence of bounding surfaces within cores of nebkhas and the development of yardangs attest the undersaturated flow conditions. The main region of eolian accumulation is the central part of the sand sheet where sand

Wind ripple strata

Subaqueous ripple strata

Mud cracks

Roots

Bioturbation

Deformed strata

OSL sample

c z vf f m c vc g

sand

OSL: Optically stimulated luminescence.
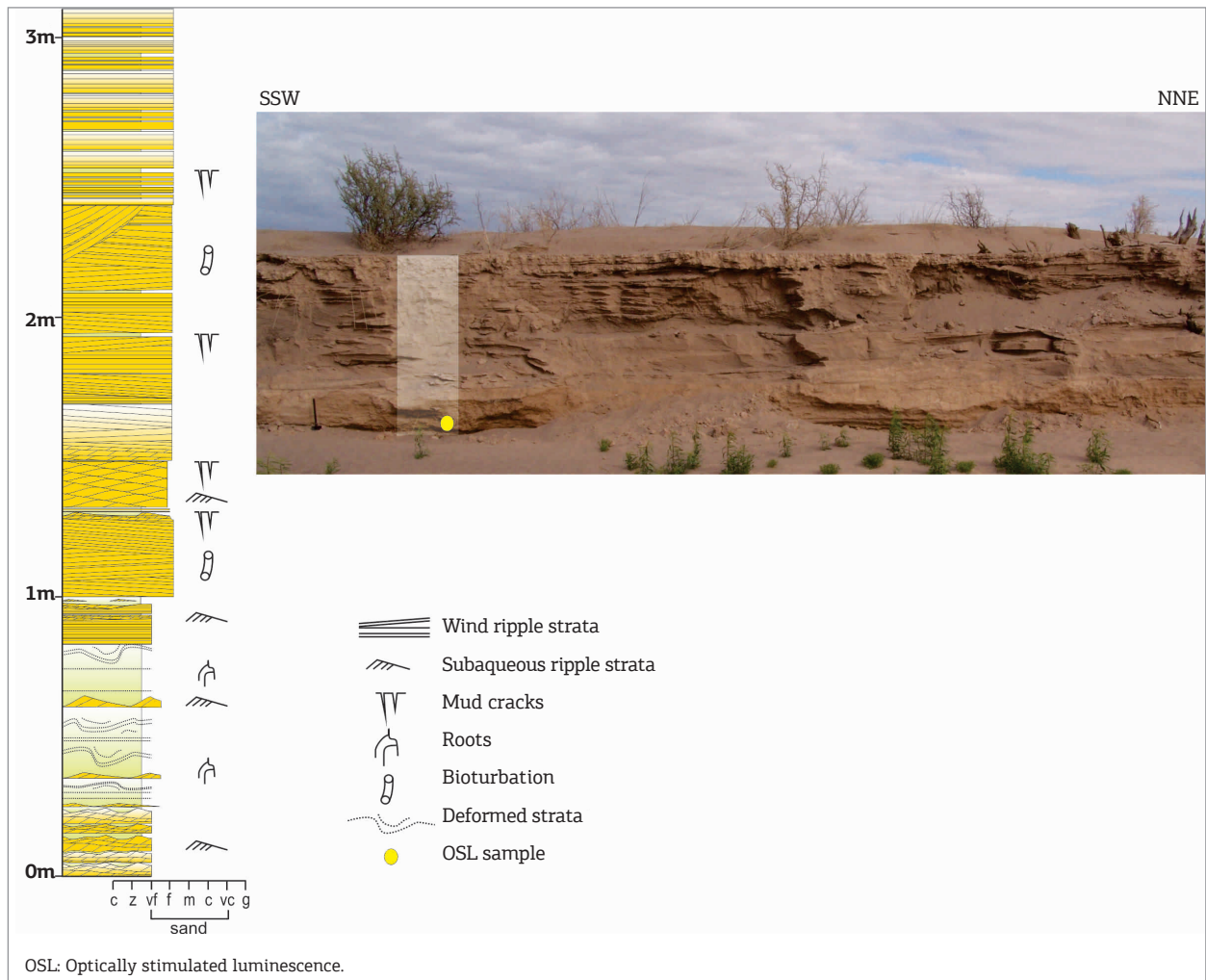
Figure 13. Stratigraphic section measured in the central part of the sand sheet showing the vertical interbedding of eolian and subaqueous deposits.

has accumulated to in excess of 4 m of thickness and is largely stabilized by vegetation. The nebkhas that are almost fully stabilized by vegetation in this region have accumulated vertically as non-migratory bedforms, as sediment is trapped by the stabilizing influence of vegetation. The widespread mud laminae, which cover eolian sand deposits at the central and south sand sheet parts and are a recurrent sedimentary feature in stratigraphic section, are an important factor that protects the surface from deflation and thus enables accumulation of sedimentary strata. Surface cementation has contributed to accumulation of sedimentary strata in the south, whereas, in the north, the minor eolian accumulation has been formed by mud deposition and aerodynamic deceleration of the wind, as it enters into small topographic depressions.

The long-term preservation of the Upper Tulum eolian sand sheet accumulations is attributed to tectonically-induced subsidence and burial. The high rates of sedimentation have enabled the continuous burial of the geological bodies, and the progressive creation of the preservation space in the tectonic active subsiding Tulum depression has enabled the accumulations be gradually placed beneath the level of deflation, thereby protecting the accumulated strata from future erosion and reworking (Kocurek 1999).

ACKNOWLEDGMENTS

REFERENCES

Ahlbrandt T.S. & Fryberger S.G. 1981. Sedimentary features and significance of interdune deposits. *In:* Etheridge F.G. & Flore R.M. (eds.). *Recent and ancient nonmarine depositional environments*: models for exploration, v. 31. Tulsa, SEPM Special Publication, p. 293-314.

Anderson R.S. 1987. A theoretical model for aeolian impact ripples. *Sedimentology*, **34**(5):943-956.

Bagnold R.A. 1941. *The physics of blown sand and desert dunes*. London, Methuen and Company, 265 p.

Basilici G. & Dal' Bó P.F.F. 2014. Influence of subaqueous processes on the construction and accumulation of an aeolian sand sheet. *Earth Surface Processes and Landforms*, **39**(8):1014-1029.

Clemmensen L.B. & Abrahamsen K. 1983. Aeolian stratification and facies association in desert sediments, Arran Basin (Permian), Scotland. *Sedimentology*, **30**(3):311-339.

Forman S.L., Tripaldi A., Ciccioli P.L. 2014. Eolian sand sheet deposition in the San Luis paleodune field, western Argentina as an indicator of a semi-arid environment through the Holocene. *Palaeogeography, Palaeoclimatology, Palaeoecology*, **411**:122-135.

Fryberger S.G., Ahlbrandt T.S., Andrews S. 1979. Origin, sedimentary features and significance of low-angle aeolian "sand sheet" deposits, Great Sand Dunes National Monument and vicinity, Colorado. *Journal of Sedimentary Petrology*, **49**(3):733-746.

Fryberger S.G., Hesp P., Hastings K. 1992. Aeolian granule ripple deposits, Namibia. *Sedimentology*, **39**(2):319-331.

Fryberger S.G. & Schenk C.J. 1988. Pin stripe lamination: a distinctive feature of modern and ancient eolian sediments. *Sedimentary Geology*, **55**(1-2):1-15.

Glennie K.W. 1970. *Desert sedimentary environments*. Developments in Sedimentology, v. 14, Amsterdam, Elsevier, 222 p.

Goodall T.M., North C.P., Glennie K.W. 2000. Surface and subsurface sedimentary structures produced by salt crusts. *Sedimentology*, **47**(1):99-118.

Goudie A.S. 2007. Mega-yardangs: a global analysis. *Geography Compass*, **1**(1):65-81.

Hummel G. & Kocurek G. 1984. Interdune areas of the Back-Island dune field, North Padre-Island, Texas. *Sedimentary Geology*, **39**(1-2):1-26.

Hunter R.E. 1977. Basic types of stratification in small eolian dunes. *Sedimentology*, **24**(3):361-387.

Kocurek G. 1981. Significance of interdune deposits and bounding surfaces in aeolian dune sands. *Sedimentology*, **28**(6):753-780.

Kocurek G. 1999. The Aeolian rock record (Yes, Virginia, it exists, but it really is rather special to create one). *In:* Goudie A.S. & Livingstone I. (eds.). *Aeolian environments, sediments and landforms*. Chichester, John Wiley and Sons, p. 239-259.

Kocurek G. & Fielder G. 1982. Adhesion structures. *Journal of Sedimentary Petrology*, **52**(4):1229-1241.

Kocurek G. & Havholm K.G. 1993. Eolian sequence stratigraphy - a conceptual framework. *In:* Weimer P. & Posamentier H. (eds.). *Siliciclastic sequence stratigraphy*. Recent developments and applications, v. 58. Tulsa, AAPG Memoir, p. 393-409.

Kocurek G. & Lancaster N. 1999. Aeolian system sediment state: theory and Mojave Desert Kelso dune field example. *Sedimentology*, **46**(3):505-515.

Kocurek G. & Nielson J. 1986. Conditions favourable to the formation of warm-climate aeolian sand sheets. *Sedimentology*, **33**(6):795-816.

Kocurek G., Townsley M., Yeh E., Havholm K., Sweet M.L. 1992. Dune and dune field development on Padre Island, Texas, with implications for interdune deposition and water-table-controlled accumulation. *Journal of Sedimentary Petrology*, **62**(4):622-635.

Köppen W. 1948. *Climatologia*: con un estudio de los climas de la tierra. Panuco, Fondo de Cultura Económica, 478 p.

Laity J.E. 1994. Landforms of aeolian erosion. *In:* Abrahams A.D. & Parsons A.J. (eds.). *Geomorphology of desert environments*. London, Chapman and Hall, p. 506-535.

Lancaster N. & Teller J.T. 1988. Interdune deposits of the Namib Sand Sea. *Sedimentary Geology*, **55**(1-2):91-107.

Langford R.P. 1989. Fluvial-aeolian interactions: Part I, modern systems. *Sedimentology*, **36**(6):1023-1035.

Langford R.P. 2000. Nabkha (coppice dune) fields of south-central New Mexico, U.S.A. *Journal of Arid Environments*, **46**(1):25-41.

Langford R.P. & Chan M.A. 1989. Fluvial-aeolian interactions: Part II, ancient systems. *Sedimentology*, **36**(6):1037-1051.

Lloret G. & Suvires G.M. 2006. Groundwater basin of the Tulum Valley, San Juan, Argentina: a morphohydrogeologic analysis of its central sector. *Journal of South American Earth Sciences*, **21**(3):267-275.

Meigs A., Krugh W.C., Schiffman C., Vergés J., Ramos V.A. 2006. Refolding of thin-skinned thrust sheets by active basement-involved thrust faults in the Eastern Precordillera of western Argentina. *Revista de la Asociación Geológica Argentina*, **61**(4):589-603.

Milana J.P. 2009. Largest wind ripples on Earth? *Geology*, **37**(4):343-346.

Milana J.P., Bercowski F., Jordan T. 2003. Paleoambientes y magnetoestratigrafía del Neógeno de la Sierra de Mogna, y su relación con la Cuenca de Antepaís Andina. *Revista de la Asociación Geológica Argentina*, **58**(3):447-473.

Milana J.P. & Ruzycki L. 1999. Alluvial-fan slope as a function of sediment transport efficiency. *Journal of Sedimentary Research*, **69**(3):553-562.

Mountney N.P. 2006. Eolian facies models. *In:* Posamentier H.W. & Walker R.G. (eds.). *Facies models revisited*, v. 84. Tulsa, SEPM Special Publication, p. 19-83.

Mountney N.P. & Russell A.J. 2004. Sedimentology of cold-climate aeolian sandsheet deposits in the Askja region of northeast Iceland. *Sedimentary Geology*, **166**(3-4):223-244.

Mountney N.P. & Russell A.J. 2006. Coastal aeolian dunefield development and response to periodic fluvial inundation, Sólheimasandur, southern Iceland. *Sedimentary Geology*, **192**:167-181.

Mountney N.P. & Russell A.J. 2009. Aeolian dune-field development in a water table-controlled system: Skeidararsandur, Southern Iceland. *Sedimentology*, **56**(7):2107-2131.

Mountney N.P. & Thompson D.B. 2002. Stratigraphic evolution and preservation of aeolian dune and damp/wet interdune strata: an example from Triassic Helsby Sandstone Formation, Cheshire Basin, UK. *Sedimentology*, **49**(4):805-833.

Murray A.S. & Wintle A.G. 2000. Luminescence dating of quartz using an improved single-aliquot regenerative-dose protocol. *Radiation Measurements*, **32**(1):57-73.

NASA - National Aeronautics and Space Administration. 2000. Landsat Program. Landsat ETM+ images, S-19-30_2000. Available from: http://zulu.ssc.nasa.gov/mrsid/. Accessed on 06.12.2010.

Olsen H., Due P.H., Clemmensen L.B. 1989. Morphology and genesis of asymmetric adhesion warts - a new adhesion surface structure. *Sedimentary Geology*, **61**(3-4):277-285.

Pereyra B.R. 2000. *Clima de la provincia de San Juan, Argentina.* Recursos y problemas ambientales de la zona árida. Andalucía, Programa Cooperativo Junta Gobierno Andalucía, p. 71-78.

Rubin D.M. 1987. *Cross-bedding, bedform and paleocurrents*, v. 1. Tulsa, SEPM Concepts in sedimentology and paleontology, 187 p.

Sharp R.P. 1963. Wind ripples. *Journal of Geology*, **71**:617-636.

SMA - Servicio Meteorológico Nacional. 2014. Estadísticas Climatológicas 1973-2013. Available from: http://www.tutiempo. net/clima/San_Juan_Aerodrome/873110.htm. Accessed on 06.26.2014.

Suvires G.M. 2004. Distribución de los suelos en función del relieve y de la neotectónica en la región sureste de la provincia de San Juan. *Revista de la Asociación Geológica Argentina*, **59**(3):376-384.

Tengberg A. & Chen D. 1998. A comparative analysis of nebkhas in central Tunisia and northern Burkina Faso. *Geomorphology*, **22**(2):180-192.

Tripaldi A. & Forman S.L. 2007. Geomorphology and chronology of Late Quaternary dune fields of western Argentina. *Palaeogeography, Palaeoclimatology, Palaeoecology*, **251**(2):300-320.

Zárate M. & Tripaldi A. 2012. The aeolian system of central Argentina. *Aeolian Research*, **3**(4):401-417.

Arquivo digital disponível on-line no site www.sbgeo.org.br